



Full Text View

[Volume 30, Issue 6 \(June 2000\)](#)

Journal of Physical Oceanography

 Article: pp. 1207–1222 | [Abstract](#) | [PDF \(382K\)](#)

Decadal Changes along an Indian Ocean Section at 32°S and Their Interpretation

Nathaniel L. Bindoff

Antarctic CRC, University of Tasmania, Hobart, Tasmania, Australia

Trevor J. McDougall

Antarctic CRC, University of Tasmania, and CSIRO Division of Marine Research, Hobart, Tasmania, Australia

(Manuscript received March 25, 1998, in final form June 25, 1999)

DOI: 10.1175/1520-0485(2000)030<1207:DCAAIO>2.0.CO;2

ABSTRACT

In the Indian Ocean subtropical gyre, historical temperature, salinity, and oxygen data with a median date of 1962 are compared with a hydrographic section taken at a mean latitude of 32°S in October–November 1987. Significant basinwide changes in all three hydrographic fields are observed below the mixed layer. On isobaric surfaces the main changes are (i) a warming of the upper 900 dbar of the water column with a maximum change in the sectional mean of 0.5°C, (ii) a freshening between 500 and 1500 dbar with a maximum freshening of 0.05 psu, and (iii) a pronounced decrease in oxygen concentration between 300 and 1000 dbar.

Examination of water mass properties shows that very significant water mass changes have occurred. On isopycnals subantarctic mode water (SAMW) and Antarctic Intermediate Water (AAIW) have freshened and cooled. Both of these water masses are on average deeper in 1987. Using the analysis of [Bindoff and McDougall \(1994\)](#), the changes of temperature at constant depth and at constant density are used to show that the water mass changes can most simply be explained by a surface warming in the source region of SAMW and by increased precipitation in the source region of AAIW.

The decrease in oxygen concentration can be explained simply by a slight slowing of the subtropical gyre allowing more time for biological consumption to decrease the oxygen concentration by water parcel translation from the formation area to the observation point. Estimates show that over the last 25 years there is an apparent decrease of the gyre spin rate

Table of Contents:

- [Introduction](#)
- [The data and data interpolation](#)
- [Observed temperature](#)
- [Observed changes in water](#)
- [Application of pure warming](#)
- [Discussion](#)
- [REFERENCES](#)
- [APPENDIX](#)
- [TABLES](#)
- [FIGURES](#)

Options:

- [Create Reference](#)
- [Email this Article](#)
- [Add to MyArchive](#)
- [Search AMS Glossary](#)

Search CrossRef for:

- [Articles Citing This Article](#)

Search Google Scholar for:

- [Nathaniel L. Bindoff](#)
- [Trevor J. McDougall](#)

of about 20% at the depth levels of SAMW; the estimated spin rate change decreases almost linearly with greater depth to zero at the oxygen minimum in Indian Deep Water (IDW). Below IDW the observed changes in oxygen concentration (and also the changes of temperature and salinity) are associated with the upward movement of isopycnals with no significant water mass change. The differences in temperature and salinity in the SAMW and AAIW are consistent with the relatively young age of these water masses inferred from CFC data.

1. Introduction

Recent results from the Tasman Sea ([Bindoff and Church 1992](#)) and the South Pacific ([Johnson and Orsi 1997](#)) have shown significant changes in the water mass properties of the upper ocean, particularly of subantarctic mode water (SAMW) and Antarctic Intermediate Water (AAIW), over the last 30 years. These authors concluded that the observed cooling and freshening on SAMW neutral surfaces were consistent with the warming of surface waters in the formation regions. These results from the ocean interior are supported by the observed increase in ocean surface temperatures. Surface warming has occurred since the 1950s over much of the Southern Ocean in the region north of the Subantarctic Front ([Bottomley et al. 1990](#)).

In this paper we increase the spatial coverage of these earlier results by examining temperature and salinity data for the Indian Ocean and extend the analysis to oxygen data. We use a zonal hydrographic section across the whole of the Indian Ocean taken in October–November 1987 ([Toole and Warren 1993](#)) with an average latitude of 32°S and the best available historical hydrographic data between 24° and 40°S, taken mostly in the 1950s and 1960s, with the aim of determining whether differences in water masses and circulation have occurred.



This paper describes and applies a simple water-mass model ([Bindoff and McDougall 1994](#)) to interpret the observed changes of temperature and salinity on pressure and neutral density surfaces in the ocean in terms of changes in atmospheric forcing in water mass source regions. This model is successful in describing the water mass changes and takes into account the role of changes in heating, precipitation minus evaporation, and winds on the water column.

The overall structure of this paper is as follows. The data and analysis techniques are described first followed by a presentation of the observed changes in the temperature, salinity, and oxygen fields on pressure surfaces ([section 3](#)) and isopycnals ([section 4](#)). [Section 5](#) applies the method of [Bindoff and McDougall \(1994\)](#) to infer how the surface forcing may have changed in the outcrop region. [Section 6](#) concludes the paper.

2. The data and data interpolation

a. Data

The historical hydrographic data used in this paper are derived from two sources: (i) the *Southern Ocean Atlas* ([Gordon et al. 1982](#)) and (ii) the hydrographic database of J. Reid (1994, personal communication) for the Indian Ocean. Both of these atlases are for a similar period (1930–1980) and jointly cover the region centered on 32°S from 40°S to 24°S. The hydrographic data from these atlases are mainly Nansen bottle data and were specifically edited for duplicates, quality, and those profiles that covered the whole water column.

There are a total of 451 casts in the combined historical dataset that met the final selection criteria ([Fig. 1](#) ) with the most intensive observational period occurring in the period from 1959 to 1966 (approximately 360 casts). Weaker side clusters exist in the late 1930s and 1970s, and these clusters represent only 22% of the observations (approximately 90). However, these side clusters are important in achieving the reasonable spatial coverage shown in [Fig. 1](#) . The mean date of all the casts is 1960 and the standard deviation is 10 years. The median date of the casts is 1962; quite close to the mean age. Thus, for the interpretation of the differences in the hydrographic fields, the time interval is 25 ± 10 years.

Surprisingly, the most common month in the historical data is July, resulting from the cruise along 32°S by the RV *Atlantis* (1965). The months from January to June (except March) all tend to have significantly more observations than the period August through December. March has the least observations with slightly less than 20 casts. When the historical data are grouped by month, the mean month is June (austral winter). Thus, the historical data can be considered to represent earlier times in the annual cycle than the synoptic section (Oct–Nov).

The recent hydrographic section consists of 109 CTD casts with an average latitude of 32°S and was obtained in October–November of 1987. Because of the complex seafloor topography of the Indian Ocean, the section was designed to cross normal to each of five major ridge systems. Consequently, this section has significant northward and southward

excursions along the cruise track making the most southerly latitude at 34°S and most northerly latitude at 29°S. For this comparison the best historical data come from the earlier zonal sections at 32°S taken from the RV *Discovery* (April 1936) and *Atlantis* (July 1965). However, [Fig. 1](#) shows that there are sufficient historical data near the recent section to make this comparison worthwhile.

In contrast to the historical data the recent hydrographic data are continuous profiles of temperature, salinity, and oxygen measurements, calibrated using water samples from a 24-bottle sampler. The accuracy of these temperature, salinity, and dissolved oxygen measurements is 0.002°C, 0.003 psu, and 0.02 ml l⁻¹ respectively ([Cook et al. 1992](#)).

Although the accuracy of individual salinity measurements is quite high, there are possible systematic differences between the two datasets. The salinities in the historical data are ppt, while the 1987 data are all based on the 1978 Practical Salinity Scale (psu). [Mantyla \(1987\)](#) has documented some of the differences in changing from ppt to pss in addition to the subtle changes associated with variations in standard seawater. These biases could be as large as 0.01 psu.

Biases that could have occurred between the historical and recent oxygen data because of differences in the titration methods are unknown. Here we are guided by the estimates of the noise in historical oxygen data to determine their accuracy (discussed in the next section).

b. Data interpolation

To make the comparison between the two datasets, the spatially irregular historical data are interpolated to the exact locations of the recent hydrographic section ([Fig. 1](#)). The interpolation of the historical data uses a combination of empirical orthogonal functions (EOF) and objective mapping ([Fukumori and Wunsch 1991](#); [Bindoff and Wunsch 1992](#)).

The main differences of the interpolation techniques used in this paper from the earlier papers is in the estimation of the a priori mean and choice of EOFs. Here, the a priori mean field is found by fitting low-order polynomials as a function of latitude to the hydrographic data at each of the 38 standard depths. This mean field estimate is an improvement over the approach adopted by [Fukumori and Wunsch \(1991\)](#) since it explicitly removes the strong north–south gradients in the fields prior to normalization of the data.

The EOFs are found using the so-called Form-2 modes, where each normalized property from an individual cast is grouped together in a single column prior to constructing the property–depth covariance matrix. See [Bindoff and Wunsch \(1992\)](#) for a discussion of the exact form of this matrix and the estimation of the a priori noise. The three properties are normalized by the a priori noise ([Fig. 2](#)) at each of the 38 standard depths. There are 114 (3 × 38) nonzero eigenvalues of which 15 were retained in the interpolation. For the objective mapping of the property–depth EOFs a horizontal length scale of 400 km was used for each of the 15 selected spatial eigenvectors and this scale is significantly longer than the average separation between casts in the historical dataset. So, although the data are analyzed on standard depths in contrast to mapping directly on density surfaces ([Lozier et al. 1994](#)), tests of the mapped water masses show that for above 3500 dbar they are well preserved.

The discussion of the differences fields between the historical data and the synoptic section emphasizes the results from the upper 3500 dbar of the water column. The analysis of the residuals (normalized by the a priori noise) between the mapped historical data and the unmapped historical data show that the mapping technique fails for the depths greater than 3500 dbar. This failure occurs because the historical data are too few and are distributed over complex bottom topography that breaks the mapping domain into small discrete basins. These basins, each with their own distinct water masses and currents, violates the underlying assumption in the mapping process of horizontal statistical homogeneity. However, analysis of the residuals between the mapped data and observations above 3500 dbar showed that the interpolated fields were statistically consistent with the a priori noise and were free of bias. The interpolated historical data to the 32°S section were then differenced with the 1987 data on pressure and density surfaces.

3. Observed temperature, salinity, and oxygen changes on pressure surfaces

For describing the differences of temperature, salinity, and oxygen it is useful to characterize the four most important water masses observed along 32°S ([Table 1](#)). In this region, along the 32°S section, SAMW at a depth range of 410–830 dbar is characterized by a potential temperature range between 6° and 14°C ([McCartney 1977](#)). Below SAMW, the salinity minimum that characterizes AAIW is found, with an average salinity and potential temperature of 34.47 psu, 4.6°C, and at an average depth of 1100 dbar. The Indian Deep Water (IDW) is characterized by an oxygen minimum and is defined by an average concentration, salinity, temperature, and depth of 3.9 ml l⁻¹, 34.62 psu, 3.0°C, and 1600 dbar. Last, Lower Circumpolar Deep Water (LCDW) is characterized by a salinity maximum, ultimately of North Atlantic origin, with an average salinity, temperature, and depth of 34.76 psu, 1.79°C, and 2700 dbar. Note that our water mass definitions here differ slightly from those of [Robbins and Toole \(1997\)](#).

The differences between the 32°S section and the mapped historical data for temperature, salinity, and oxygen all show basinwide differences on isobaric surfaces (Figs. 3, 4, 5). Because of the relatively sparse spatial distribution of the historical observations, the only differences that are important are those on scales much larger than the mapping scales used to project the historical observations onto the 32°S section (i.e., >400 km).

The temperature difference field (Fig. 3) shows a consistent warming of the SAMW across the whole Indian Ocean, except near 50°E where there is some possible cooling. Below this mode water, at the AAIW depth (average depth 1100 dbar), the temperature difference field has a quite different pattern. In the east, from 65°E to Australia, the temperature has decreased very slightly while in the west, from 45° to 65°E the temperature has decreased more strongly. The larger cooling to the west on isobars in the depth range of the salinity minimum water is significant at the 90% confidence level, and the implied change in slope of isopycnals suggests a possible change in the circulation of the gyre.

Below the AAIW in the Indian Deep Water (1600 dbar) the temperature differences show a cooling in the west of the section and a temperature increase in the east. The areal extent of this cooling region increases with depth below the AAIW down to 3500 dbar.

The salinity differences on isobars show a different pattern to the temperature differences. From Africa to Australia, the shallower depths of the SAMW layer (200–400 dbar) show a basinwide increase in salinity (Fig. 4). In the lower layers of the SAMW (400–750 dbar) from Africa to 70°E the salinity differences show a slight salinity increase on average. In contrast, from 70°E to Australia (slightly more than half of the section) the salinity has decreased at these depths. Although there are “spots” of positive differences, the salinity differences on isobars from 1100 to 2700 dbar show a broad basin-scale decrease in salinity. This depth range includes the AAIW, IDW, and LCDW water masses.

One of the tests of the quality of the oxygen data (both historical and synoptic) is the small size of the oxygen differences in the mixed layer (<100 dbar) where the water is presumed to be near saturation. The historical data were mainly obtained during the month of June and thus are likely to have a lower oxygen saturation compared with the late winter period of October when the synoptic section was obtained (Fig. 6). The mean difference across the whole section is 0.1 ml l^{-1} consistent with the October section being colder and hence with a higher concentration. The mixed layer temperature in the synoptic section is, in fact, cooler by 0.5° (Fig. 6) and is sufficient to explain 0.05 ml l^{-1} of the mixed layer oxygen difference. This result suggests that an upper limit to any systematic oxygen bias in the oxygen data is less than 0.05 ml l^{-1} ; $\frac{1}{4}$ of the a priori noise.

At the level of SAMW the oxygen data on isobars show a very striking decrease in oxygen concentration across the whole section between 1962 and 1987 (Fig. 5). This basinwide decrease in oxygen concentration extends to just above the salinity minimum at 1000 dbar. The decrease in oxygen concentration is strongest in the western half of the section and is weaker in the eastern half. For waters from the depth of the AAIW through to the depth of the IDW (1100–1600 dbar) the oxygen differences have a more bimodal distribution. From Africa to 70°E the oxygen concentration has increased weakly, while from 70°E to Australia the oxygen signal has tended to decrease. Below the oxygen minimum the oxygen concentration has a basinwide increase except in the relatively small region between 55° and 78°E where there is a decrease.

The observed differences in the temperature, salinity, and oxygen fields on isobars have large spatial scales. Because of the sparsity of historical data in both time and space, the observed differences with the greatest significance are the basinwide averages of each of these tracer fields (Fig. 6). The error bars shown are 90% confidence intervals. These confidence intervals are based on a simple *t*-test criteria and take into account the number of degrees of freedom in the historical data at each depth, the error in differencing the two fields, and the a priori noise (Fig. 2). The degrees of freedom are estimated from the total number of data near the section and at the surface is about 100 reducing with depth. The a priori noise takes into account the unresolved natural variability due to mesoscale eddies and to a limited extent seasonal changes.

Based on the 90% confidence intervals the surface waters, SAMW, AAIW, and IDW show significant basinwide differences. The apparent differences in the surface waters can be explained by aliasing the seasonal signal between the synoptic section and historical data. The October–November data of the RSS *Charles Darwin* reflect the austral spring temperature, salinity, and oxygen fields while the most common month in the historical data is July, representing the winter ocean fields. The expected mixed layer temperature difference between these months can be estimated from a seasonal atlas of the surface heat flux, based on the monthly averages of the ECMWF model output from 1986–89 (Barnier et al. 1995) and a very simple model of the mixed layer. Assuming no exchange between the mixed layer and ocean interior and neglecting horizontal advection, the seasonal heat flux difference (approximately 100 W m^{-2}) shows that the synoptic section in the mixed layer (<100 dbar) should be approximately 0.5°C cooler than the historical section, as observed.

The surface salinities on the 1987 voyage are higher than the July 1962 mean by 0.07 psu on average. The pattern of precipitation minus evaporation is poorly known in this region because there are few observations. However, forecast model

predictions of the $P - E$ pattern from the Bureau of Meteorology (Australia) (Bourke et al. 1991) show that precipitation minus evaporation ($P - E$) pattern at the latitude of these sections is more negative during winter months (JJA) than during the summer months (DJF). The average increase between winter and summer is approximately 200 mm yr^{-1} and implies that the mixed layer during the synoptic cruise should be more salty than that observed in the historical section. Assuming no exchange between the mixed layer and the ocean interior, this difference in $P - E$ will cause a maximum rise in the salinity of about 0.07 psu. This crude calculation agrees surprisingly well with the observed difference between the synoptic section and the historical data.

The consistency of the mixed layer differences in temperature, salinity, and oxygen fields with the surface heating and $P - E$ patterns, and the relatively small size of these seasonal differences gives us confidence that the larger subsurface differences are not aliased seasonal variations.

The largest temperature difference occurs below the mixed layer, with a sectional average warming of 0.5°C at a depth of 220 dbar. This warming extends coherently over the depth range occupied by SAMW. At AAIW depths, there is a pronounced basinwide cooling of 0.25°C . Between 1500 and 3500 dbar (the limit of good interpolation of the historical data) the temperature has decreased evenly by about 0.05°C . The basinwide salinity changes on isobars show weak changes in the SAMW (relative to the confidence interval). However, below the SAMW there is a striking decrease in salinity on isobars with the maximum change of almost 0.05 psu at the depth of the salinity minimum (1100 dbar). Below the AAIW, the salinity differences are small compared to the confidence intervals. The basinwide oxygen differences show a strong decrease particularly in the depth range of SAMW (between 300 to 800 dbar) and a strong increase below IDW (>2500 dbar).

A significant steric sea-level change is caused by these differences of temperature and salinity. The depth-integrated steric rise consists of -0.007 m contribution for waters from 3000 to 1000 dbar and 0.042 m for waters above 1000 dbar giving a total depth-integrated rise of 0.035 m or 1.6 mm yr^{-1} . This estimate of the sea-level rise compares well with the estimated global sea-level rise for the last century of 1.8 mm yr^{-1} (Douglas 1991).

4. Observed changes in water mass properties

The question arises whether these observed changes on isobars reflect differences in the watermass properties and hence ocean-atmosphere exchanges or are simply the result of ocean dynamics. It is conceivable, for instance, that the temperature differences could have been created by a relatively small lateral movement of the subtropical gyre. Indeed, the synoptic 32°S section is very nearly in the middle of the Indian subtropical gyre, and therefore any north-south excursion of the gyre would cause both a decrease in temperature (not observed) and a decrease in salinity (also not observed) on isobars. Thus, in this case it is relatively easy to rule out N-S lateral shifts of the subtropical gyre as an explanation of the observed changes on isobars (and density surfaces).

Instead of using the more familiar σ_θ surfaces we use neutral density, γ^n . Neutral density is the density variable that corrects for the compressible nature of seawater and is defined in such a way that it is always constant along neutral surfaces (Jackett and McDougall 1997). Along the 32°S section it is a simple matter to convert from neutral density to any σ_θ , σ_1 , and σ_2 density because the correlation between neutral density and σ is almost perfectly linear (Table 2).

However, the slope and intercept describing the relation between σ and γ^n are only valid in regions close to the 32°S section. In Table 1 it can be seen that for SAMW σ_θ is about 0.1 kg m^{-3} less than the equivalent defining γ^n surfaces.

The differences of water masses on neutral surfaces (Fig. 7) are even more significant than the changes on isobars. The average change of salinity and potential temperature on neutral density surfaces and the $S-\theta$ curve shows that throughout SAMW and AAIW the waters are now cooler and fresher. The maximum decrease in temperature and salinity occurs at 26.8 kg m^{-3} with an average depth of 450 dbar, with a cooling and freshening of 0.54°C and 0.13 psu (Fig. 7b). At the salinity minimum, around 27.45 kg m^{-3} , there is a decrease of 0.33°C and 0.06 psu .

In addition the depths of the density surfaces increased on average for all densities above 27.77 kg m^{-3} (Fig. 8a). The largest depth change occurs in density range $26.7\text{--}27.1 \text{ kg m}^{-3}$ (410–830 dbar), with density surfaces displaced downward by a sectional mean of 70 m. The nonuniform depth changes show that SAMW is now thicker and that AAIW is now thinner (Fig. 8a). The relative potential vorticity change (h'/h , where h is the distance between neutral density surfaces) has decreased by 25% at $\gamma^n = 26.7 \text{ kg m}^{-3}$ and increased by 25% in the density range $27.1\text{--}27.4 \text{ kg m}^{-3}$. Below AAIW the relative potential vorticity changes are small, less than 5%.

On neutral density surfaces, the difference in potential temperature (Fig. 9) shows a remarkably consistent pattern of cooling across the whole section, even more regular than the warming pattern shown in Fig. 3. Mesoscale eddies and other sources of oceanographic noise tend to introduce large vertical excursions of density surfaces (and strong temperature fluctuations on isobars), whereas the changes on the density surfaces result from the integration of air–sea exchange anomalies of long timescales and therefore tend to be smoother. This cooling on neutral surfaces in the main thermocline is consistent with warming on isobars (see appendix A). We do not show the across-basin changes for the other fields due to a lack of space, but they also show coherent basinwide patterns in water properties reflected in the section-averaged differences shown below.

In addition to the average difference in potential temperature on density surfaces (θ'_n) there is also a gradient of change across the basin. The differences in SAMW potential temperature (θ'_n) are large in the eastern part of the basin, even larger about 100°–110°E, and smaller to the west. For AAIW ($\gamma^n \sim 27.4 \text{ kg m}^{-3}$) where there is broadscale cooling on density surfaces over the entire basin, the larger changes tend to occur between 60° and 90°E.

This distribution of the differences of potential temperature on density surfaces (θ'_n) is also consistent with the circulation of SAMW and AAIW. SAMW moves north from its source region and crosses the section most strongly in the eastern part of the section. It continues around the gyre north of the section to return south in the Agulhas Current. This pattern of circulation suggests that the SAMW tend to be younger in the eastern part of the section. This interpretation is confirmed by the higher oxygen concentrations in the east (Toole and Warren 1993) and by the distribution and apparent age from chloro-fluorocarbon measurements obtained on the 1987 cruise (Fine 1993). For AAIW, the apparent ages estimated from the CFCs showed that the youngest waters were west of 72°E, in the same basin as the larger changes that are observed on this density horizon.

5. Application of pure warming, pure freshening, and pure heave to the Indian Ocean

Here we use the method of Bindoff and McDougall (1994) for interpreting the observed differences in the hydrographic data on pressure and density surfaces. The approach is kinematic rather than dynamic but has the advantage of relative simplicity in understanding the observed changes in temperature and salinity. Appendix A gives an account of the underlying method used in this analysis and differences from the above paper.

The basic concept is as follows: Under global or regional warming, the flux of heat from the atmosphere into the ocean will increase. Precipitation minus evaporation will also change under these conditions, thus contributing to a change in the surface buoyancy flux. In addition, the wind stress curl is likely to change, altering the ocean circulation and the depth of density surfaces. The concepts of pure warming, pure freshening, and pure heave involve, respectively, change in one of the surface forcings, that is, (i) surface heat flux, (ii) surface precipitation minus evaporation, or (iii) wind stress curl, while holding the other two constant. In this way we seek to identify the effectiveness of each process in producing the observed changes in temperature and salinity fields. In the real ocean the response to global or regional change is likely to be a combination of these three processes. These three processes can be quantified (as described in appendix A) and relative strength of each process can be estimated using inverse methods.

The zonal averages of the differences in potential temperature and salinity on isobars, density surfaces, and by the vertical displacement of density surfaces in the mean vertical gradient form the basic data describing the three processes. These averages are weighted by the thermal expansion coefficient α and haline contraction coefficient β to form the density anomalies $\alpha\theta'_z$, $\alpha\theta'_n$, $N'\alpha\theta'_z$, $\beta S'_z$, $\beta S'_n$, and $N'\beta S'_z$ (shown in Fig. 10 and appendix A). The contribution of each term in both temperature and salinity can now be directly compared. It can be seen that in terms of density anomaly, the differences in temperature are the largest source of expansion of the water column (i.e., $\alpha\theta'_z > \beta S'_z$). It can also be seen that although the vertical displacement of the neutral surfaces is a large contribution to the change in temperature and salinity on isobars, i.e.,

$$\alpha\theta'_z \sim -\alpha N' \frac{\partial \theta}{\partial z},$$

the change in temperature (or salinity) on neutral surfaces are also important and has a higher signal-to-noise when compared with the other terms because of its small confidence interval.

The relative strength of each of the three processes can be shown on a hodograph because only two pieces of independent information are contained in the six observables. Here, we choose the two axes of the hodograph to be $R_\rho/(R_\rho - 1)\beta S'_z$ and $1/(R_\rho - 1)\alpha\theta'_z$, where R_ρ is the stability ratio. This set of axes differs from those used in Bindoff and McDougall

(1994) and in Vaughan and Molinari (1997) but has the distinct advantage that each of the three processes can be represented as vectors with constant direction (Fig. 11). It can be seen that the basinwide differences divide into two regimes. The first regime, and shallowest, corresponds to SAMW waters ($\gamma^n = 26.7\text{--}27.1 \text{ kg m}^{-3}$) where the points on the hodograph tend to lie parallel to the warming axis, although there could also be contributions from heave and freshening as well in this density range.

The second regime, corresponds to the waters surrounding the salinity minimum ($\gamma^n = 27.1$ to 27.8 kg m^{-3}). In this range of densities the potential temperature differences tend to be small, while the differences in salinity tend to be much larger causing the differences to lie along the axes representing the pure freshening process.

For the deeper depths including LCDW ($\gamma^n > 27.8 \text{ kg m}^{-3}$) the differences tend to lie parallel to the axis representing the heave process. For these layers the density anomalies are small and the confidence intervals in Fig. 10 indicate these differences are not strongly significant. However, the suggestion that LCDW water masses are unchanged and that the small observed differences (albeit barely significant) are best explained by the displacement of isopycnals is consistent with its long ventilation timescale.

The same interpretation can be found by solving Eq. (A6). Because Eq. (A6) has only two nonzero eigenvalues, it is not possible to solve uniquely for all three of the processes. There is a range of methods for solving these ill-posed systems, for example, by minimizing the norm of the process vector A^w, A^f, A^h (Menke 1984). In an earlier paper the purely underdetermined solutions were explored for similar changes in the Tasman Sea (Bindoff and McDougall 1994). Here, an ‘‘Occam’s razor’’ approach is used where Eq. (A6) is solved singly for each of the individual processes rather than for the linear combination of the three processes. The solution for a single process is overdetermined.

This approach allows the identification of neutral surfaces where each of the individual processes best explain the observed differences and thus provides the simplest interpretation of the observations. In practice the three processes are more likely to occur together. For example, in the sea-level rise model of Church et al. (1991), the surface buoyancy changed the internal density field sufficiently for it to depart from Sverdrup balance. As a result, the heave process was required, resulting in a shoaling of density surfaces across the subtropical gyres.

For the Indian Ocean, there are two density intervals where a single process tends to dominate the observed differences (Fig. 12, Table 1). For density surfaces deeper than 26.7 kg m^{-3} (410 dbar) and shallower than 27.7 kg m^{-3} , pure heave explains less than 50% of the variance in the observed differences in all six observables. The skill of pure heave in explaining these 25-yr differences is poor, suggesting that water mass changes in the source regions are playing the dominant role in the modification of the temperature and salinity structure. On neutral density surfaces between γ^n of 26.7 and 27.1 kg m^{-3} pure warming explains more than 95% of the variance and explains a greater percentage of the signal than either of the other two processes, pure freshening or pure heave. However, for most density surfaces within this regime, pure freshening also explains greater than 80% of the variance. This suggests, that while pure warming is dominant, it is likely that the freshening process also contributes to the observed changes in this density range. This warming regime corresponds primarily to the SAMW waters ventilated north of the Sub-Antarctic Front.

The second regime is defined by the density surfaces $\gamma^n = 27.1$ to 27.7 kg m^{-3} . On the $S\text{--}\theta$ diagram this regime straddles the AAIW. Here, neither pure heave nor pure warming have a role in explaining the observed differences in these single process solutions. However, pure freshening explains 75%–95% of the signal over these density layers. This result is expected, based on the shape of the $S\text{--}\theta$ curve, because the pure warming process cannot contribute to observed freshening on the neutral surfaces around the AAIW (see appendix B). In this way, the concepts of pure warming and pure freshening are based on classical water mass analysis since we are fitting three processes to the $S\text{--}\theta$ curve. Because of the shape of the $S\text{--}\theta$ curve, it is clear that pure warming and pure heave cannot play a role in decreasing the salinity at the salinity minimum to match the observed variations. The simplest interpretation remains that the only process necessary to explain the basinwide differences at this level is pure freshening.

On deeper layers ($\gamma^n > 27.9 \text{ kg m}^{-3}$, deeper than approximately 2200 dbar) below IDW the percentage variance explained drops dramatically. More importantly the formal confidence intervals on each process becomes large relative to the signal, and thus the estimated strengths of the three processes are not significant on these deeper layers (Fig. 13).

The Occam’s razor approach of taking a single process to explain the data shows quite clearly that the observed differences on any particular neutral surface can usually be explained by either pure warming or pure freshening. In regimes I and II, pure heave did not contribute significantly to the observed changes. This fact suggests that solutions to Eq. (A6) could be explored that include just pure warming and pure freshening. Such a solution (Fig. 14) is evenly determined and explains all of the variance in the observations. The Occam’s Razor solution (Fig. 13) and the evenly determined solution (Fig. 14) differ in the shallowest layers for pure freshening ($\gamma^n < 26.7 \text{ kg m}^{-3}$) and in AAIW ($\gamma^n = 27.4 \text{ kg m}^{-3}$) for

both pure warming and pure freshening processes.

The shallow layers show a slight increase in salinity on isobars, and the pure freshening process is able to adjust the solution for this feature (Fig. 10). In AAIW, the mixed warming and freshening solution shows that the freshening process is more positive (i.e., the density anomaly is more negative) and the warming process is more negative (i.e., the density anomaly is positive) than the Occam's Razor solution. This change in the solution occurs because the warming process takes into account the cooling on isobars that is observed around the salinity minimum (Fig. 6). The implication of this evenly determined solution is that the surface water associated with the formation of AAIW may have cooled as well as freshened.

The concepts of pure warming and pure freshening deal only with the subduction of changed surface temperature and salinity through changes in ocean heat flux and precipitation minus evaporation. In both of these cases, the oxygen content of the subducted water is fixed by the saturation of surface waters. Following the same arguments as described in appendix A for the pure warming or pure freshening processes, no difference in oxygen content on pressure surfaces is expected. In the case of pure heave, water mass properties are unchanged and thus the difference in oxygen concentration on neutral surfaces is also zero. Figure 6c shows the oxygen difference profile that occurs in conjunction with the observed warming. This profile is calculated allowing for the changes that the observed temperature (Fig. 6a) would have on the oxygen saturation in the surface mixed layer. This is not a complete correction since it assumes that the observed changes are precisely the changes that would have been observed in the source regions. For water above AAIW the observed increase in temperature does appreciably reduce the adjusted oxygen content. However, the differences in the adjusted oxygen values are still significant at the 90% confidence level between 200 and 900 dbar and slightly enhanced below 900 dbar to the oxygen minimum where the water column has cooled.

These significant oxygen differences on isobaric and density surfaces (Fig. 8b) suggests that there has been a change in the circulation rate of the subtropical gyre or that the heave process has moved isopycnals within the water column. Oxygen saturated waters are subducted and carried into the interior along isopycnals where they mix through mechanical processes. More importantly the oxygen is slowly consumed by biological processes. If it is assumed that the mixing rate is unchanged, these differences reflect a net increase in the oxygen consumed by biological processes. If the oxygen consumption rate is unchanged, the observed oxygen decrease implies that fluid parcels took longer to arrive at the synoptic section in 1987 than 1962 or that the region of subduction was farther away in 1987. It is possible to get an idea of the timescale changes by calculating the apparent age ratio. The apparent age ratio ($\Delta t/\tau$) is given by

$$\frac{\Delta t}{\tau} = \frac{\ln(C_o/C_i) - \ln(C_n/C_i)}{\ln(C_n/C_i)}, \quad (1)$$

where C_i , C_n , and C_o are the initial surface saturation (dependent on temperature), the new concentration observed on the 1987 section, and the old concentration of oxygen from the historical data at the observation point. This equation has assumed that the oxygen consumption rate is unchanged along the path that the fluid has taken from the source region to the observation point. Here τ is the travel time for fluid parcels from the subduction region to the observations and Δt is the change in time taken by the fluid to reach the observation point. The value of the apparent age ratio is that it is independent of the numerical value of the biological consumption rate.

This simple model shows that the apparent age of water parcels has increased by approximately 20% at 300 dbar. The age changes decreases roughly linearly to zero at approximately 1900 dbar (just below the oxygen minimum). This pattern of change is consistent with the warming and freshening regimes, where the total contribution of the warming or freshening to the steric sea level decreases from a maximum near 300 dbar ($\gamma^n = 26.75 \text{ kg m}^{-3}$) to a minimum near $\gamma^n = 27.75 \text{ kg m}^{-3}$ or 1600 dbar (see Fig. 13).

The point of zero apparent age difference occurs just below the oxygen minimum (at $\gamma^n = 27.76 \text{ kg m}^{-3}$ and approximately 1600 dbar) and is consistent with the idea that the oxygen minimum waters are the oldest waters within the water column and are flowing southward (Toole and Warren 1993). Thus, on the timescale of these data the oxygen minimum waters are the least likely to show changes in water mass properties.

There is some evidence from the density field that the circulation has slowed as discussed earlier. Using a reference level of 1500 dbars, the thermal wind transport across the section has been integrated westward from the eastern boundary to 45°E (i.e., away from the Agulhas Current). The cumulative transport above the oxygen minimum (1500 dbars) shows a decrease in the northward transport of the subtropical gyre of 2–8 Sv (Sv $\equiv 10^6 \text{ m}^3 \text{ s}^{-1}$) on a mean transport of 35–40 Sv or roughly 15%. These calculations are sensitive to the longitude of integration, but are broadly consistent with the inferred slow down in the spin rate of the gyre from the oxygen data.

The suggestion that the deep changes below IDW are a result of the pure heave is also supported by the change in oxygen

on neutral surfaces (Fig. 8). Below IDW ($\gamma^n > 27.6 \text{ kg m}^{-3}$ and $>2000 \text{ dbar}$) where biological consumption is low, the change in oxygen concentration on isobars is large ($>0.1 \text{ ml l}^{-1}$ in Fig. 6), whereas the change in oxygen concentration on neutral surfaces is smaller ($<0.05 \text{ ml l}^{-1}$) and is very close to the bias estimated between the historical and synoptic oxygen data. Thus, the oxygen differences observed on pressure surfaces with relatively weak changes on density surfaces below IDW and in LCDW is consistent with these deep waters undergoing pure heave.

6. Discussion

The consistency of these Indian Ocean results with the differences of temperature and salinity on neutral surfaces reported in the Tasman Sea and Southwest Pacific (Bindoff and Church 1992; Bindoff and McDougall 1994; Johnson and Orsi 1997) is striking. The data in these papers show the same warming of the SAMW, with a corresponding and very significant cooling, freshening, and deepening of isopycnals. Below the SAMW, the AAIW has freshened even more strongly than in the Tasman Sea region. The pattern of the pure warming and pure freshening as a function of γ^n is almost identical for all of these datasets [cf. Fig. 11a of Bindoff and McDougall (1994) with Fig. 12 of this paper]. Thus, the results in this paper extend the domain of the earlier results, to a significant proportion of the globe, now including the entire south Indian and South Pacific Ocean (roughly 225° of longitude).

In the Tasman Sea the AAIW is now fresher on neutral surfaces by approximately 0.03 psu. In the Indian Ocean the salinity minimum is fresher by 0.06 psu. Historical data analysis and numerical models suggest that the major formation region for AAIW is in the southeastern Pacific (McCartney 1977; England 1992) and that these waters flow eastward through Drake Passage along the Antarctic Circumpolar Current toward the Indian Ocean and Tasman Sea. With this circulation pattern the Indian Ocean should show a larger change of salinity minimum water than the Tasman Sea, and it would seem likely that the South Atlantic or eastern South Pacific should show an even larger signal of freshening.

Unfortunately no historical records exist of change of the precipitation pattern over the Southern Ocean that can confirm the implied surface freshening signal. There is a possible role for sea ice to influence the salinity of AAIW, but the observed decrease in sea ice extent since the 1950s (Jacka and Budd 1991) is relatively small. However, the observation of increased freshening for AAIW has some support from numerical models. Coupled ocean–atmosphere models for a gradual doubling of atmospheric CO_2 (Manabe et al. 1990, 1991) show that the surface waters south of the Antarctic Circumpolar Current become fresher through increased precipitation.

The warming of the SAMW in the Indian Ocean is consistent with the surface warming of the south Indian Ocean from the subtropical gyre to the Subantarctic Front for the 1950s to late 1980s (Bottomley et al. 1990). This result is also supported by other surface temperature analyses for the same region and period (Hansen and Lebedeff 1987, 1988; Jones 1988). Over most of the South Indian subtropical gyre surface temperatures have increased by 0.25°C since the 1950s. More significantly the outcrop area of SAMW, north of the Sub-antarctic Front, in both of the South Atlantic and Indian Oceans appear to have warmed by between 0.3° and 1.0°C over this same period. It is in this latitude range (45° – 55°S) that SAMW is subducted and transported northward across the hydrographic section.

The results presented here show a pattern of differences over the last two to three decades that appears consistent with the sorts of changes predicted by increasing CO_2 in coupled ocean–atmosphere models. However, new model and observational results that specifically examine climate variability on decadal time scales (Jacobs et al. 1996; Latif and Barnett 1994) also show some similarities to our observations. Further work is needed to reduce the spatial aliasing in the measurement of the subsurface temperature, salinity, and oxygen fields by further comparison of the historical data with the new WOCE hydrographic sections.

Acknowledgments

We thank the Dr. J. Toole for providing the WOCE 15 hydrographic section and Phil Reid for the analyzed GASP $P - E$ data. Comments from one anonymous reviewer, Gregory Johnson and Steve Rintoul have been very helpful in sharpening the focus of the paper. This paper is a contribution to WOCE.

REFERENCES


- Barnier, B., L. Siefridt, and P. Marchesiello, 1995: Thermal forcing for a global ocean circulation model using a three-year climatology of ECMWF analyses. *J. Mar. Syst.*, **6**, 363–380.
- Bindoff, N. L., and J. A. Church, 1992: Warming of the water column in the Southwest Pacific Ocean. *Nature*, **357**, 59–62.

- , and C. Wunsch, 1992: Comparison of synoptic and climatologically mapped sections in the South Pacific Ocean. *J. Climate*, **5**, 631–645.. [Find this article online](#)
- , and T. J. McDougall, 1994: Diagnosing climate change and ocean ventilation using hydrographic data. *J. Phys. Oceanogr.*, **24**, 1137–1152.. [Find this article online](#)
- Bottomley, M., C. K. Folland, J. Hsiung, R. E. Newell, and D. E. Parker, 1990: Global ocean surface temperature atlas: GOSTA, Tech. Rep., Meteorological Office, Bracknell, United Kingdom 1–333..
- Bourke, W., T. Hart, R. Seaman, L. Rikus, P. Steinle, M. Naughton, P. Mullenmeister, and G. Emberg, 1991: Operational global assimilation and prediction in the Bureau of Meteorology. Tech. Rep., Bureau of Meteorology Research Centre, Melbourne, Australia, 54–72..
- Church, J. A., J. S. Godfrey, D. R. Jackett, and T. J. McDougall, 1991: A model of sea level rise caused by ocean thermal expansion. *J. Climate*, **4**, 438–456.. [Find this article online](#)
- Cook, M. F., J. M. Toole, G. P. Knapp, R. A. Fine, Z. Top, and J. C. Jennings Jr., 1992: A trans-Indian Ocean hydrographic section at latitude 32°S. Data report of RRS *Charles Darwin* Cruise #29. Woods Hole Oceanographic Institution Tech. Rep., WHOI-92-07, 190 pp..
- Douglas, B. C., 1991: Global sea level rise. *J. Geophys. Res.*, **96** (C4), 6981–6992..
- England, M. H., 1992: On the formation of Antarctic Intermediate and Bottom Water in ocean general circulation models. *J. Phys. Oceanogr.*, **22**, 918–926.. [Find this article online](#)
- Fine, R. A., 1993: Circulation of Antarctic Intermediate Water in the South Indian Ocean. *Deep-Sea Res.*, **40**, 2021–2042..
- Fukumori, I., and C. Wunsch, 1991: Efficient representation of the North Atlantic hydrographic and chemical distributions. *Progress in Oceanography*, Vol. 27, Pergamon, 111–124..
- Gordon, A., E. J. Molinelli, and T. N. Baker, 1982: *Southern Ocean Atlas*. Alfred Wegener Institute, 11 pp. and 233 plates..
- Hansen, J., and S. Lebedeff, 1987: Global trends of measured surface air temperature. *J. Geophys. Res.*, **92**, 13 345–13 372..
- , and —, 1988: Global surface air temperatures: Update through 1987. *J. Geophys. Res. Lett.*, **15**, 323–326..
- Jacka, T. H., and W. F. Budd, 1991: Detection of temperature and sea-ice extent changes in the Antarctic and Southern Ocean. *Int. Conf. on the Role of Polar Regions in Global Change*, G. Weller, C. L. Wilson, and B. A. B. Severin, Eds. University of Alaska, 63–70..
- Jackett, D., and T. J. McDougall, 1997: A neutral density variable for the world's ocean. *J. Phys. Oceanogr.*, **27**, 237–263.. [Find this article online](#)
- Jacobs, G. A., H. E. Hurlburt, J. C. Kindle, E. J. Metzger, J. L. Mitchell, W. J. Teague, and A. J. Wallcraft, 1996: Decade-scale trans-Pacific propagation and warming effects of El Niño anomaly. *Nature*, **370**, 360–363..
- Johnson, G. C., and A. H. Orsi, 1997: Southwest Pacific Ocean water-mass changes between 1968/69 and 1990/91. *J. Climate*, **10**, 306–316.. [Find this article online](#)
- Jones, P. D., 1988: Hemispheric surface air temperature variations: Recent trends and an update to 1987. *J. Climate*, **1**, 654–660.. [Find this article online](#)
- Latif, M., and T. P. Barnett, 1994: Causes of decadal climate variability over the North Pacific and North America. *Science*, **266**, 634–637..
- Lozier, M., M. McCartney, and W. Owens, 1994: Anomalous anomalies in averaged hydrographic data. *J. Phys. Oceanogr.*, **24**, 2624–2638.. [Find this article online](#)
- Manabe, S., K. Bryan, and M. J. Spelman, 1990: Transient response of a global ocean–atmosphere model to a doubling of atmospheric carbon dioxide. *J. Phys. Oceanogr.*, **20**, 722–749.. [Find this article online](#)
- , R. J. Stouffer, M. J. Spelman, and K. Bryan, 1991: Transient responses of a coupled ocean–atmosphere model to gradual changes of atmospheric CO₂. Part I: Annual mean response. *J. Climate*, **4**, 785–818.. [Find this article online](#)
- Mantyla, A., 1987: Standard seawater comparisons updated. *J. Phys. Oceanogr.*, **17**, 543–548.. [Find this article online](#)
- McCartney, M. S., 1977: Subantarctic mode water. *A Voyage of Discovery*, M. Angel, Ed., Pergamon, 103–119..
- McDougall, T. J., 1987: Neutral surfaces. *J. Phys. Oceanogr.*, **17**, 1950–1964.. [Find this article online](#)


APPENDIX A

7. Pure Warming, Pure Freshening, and Pure Heave

a. Pure warming


Suppose that the heat flux across the ocean–atmosphere interface is increased and the surface mixed layer is warmed but that the pattern of $P - E$ and wind stress curl is held constant ([Fig. A1](#) ). Mixed layer fluid parcels, which would have subducted into the ocean interior along ρ_1 , now subduct into the ocean interior on the slightly less dense surface ρ_2 . The diversion of the subducting volume from the more dense ρ_1 surface to the less dense ρ_2 surface means that all the fluid between the ρ_1 and ρ_2 density surfaces is now displaced slightly downward in the water column. Note, however, that the total volume and rate of subduction between these two surfaces has remained unchanged. As a result the mean position of the fluid between these two surfaces has remained constant and, because the salinity of the subducted water parcels has been held constant in this scenario, the volume averaged salinity between the ρ_1 and ρ_2 surfaces is also unchanged.

However, because of the warming of the subducted water between these two surfaces, the volume averaged potential temperature will have increased. Thus, in this scenario, the surface warming at constant salinity followed by subduction is equivalent to warming thermocline fluid parcels at a given depth without a change in salinity on constant pressure surfaces.


This subduction scenario can also be considered on the S – θ diagram of [Fig. A1b](#) . The fluid parcel, from the original thermocline with properties S_1 , θ_1 , and density ρ_1 is warmed without change in salinity to have properties S_1 , θ_2 , and density ρ_2 . This warmed fluid parcel has the same density as the original thermocline with properties S_3 , θ_3 . Prior to the surface water warming, the volume averaged salinity and potential temperature between the two density surfaces is S_4 , θ_4 . After warming, from the discussion above, the average salinity between the two density surface is unchanged, but the volume-averaged potential temperature has now increased. As a result of this warming sequence, the volume averaged properties are S_4 , θ_5 . This averaged parcel has the same density on the original thermocline represented by S_6 , θ_6 .

This result has important implications for the interpretation of changes on density surfaces. Along a given density surface, the result of this warming scenario is that the fluid properties S_4 , θ_5 are both cooler and fresher than the original thermocline properties S_6 , θ_6 . This counterintuitive result was described by [Bindoff and McDougall \(1994\)](#) following the earlier work of [Church et al. \(1991\)](#).

b. Pure freshening

Suppose now that the mixed layer is freshened through a change in the $P - E$ pattern, while the ocean–atmosphere heat flux and wind stress curl are held constant. The same subduction argument for the pure warming case is used, except now the subducted water is fresher with potential temperature held constant ([Fig. A2](#) ).

Because the potential temperature of the subducted water parcels has been held constant in this scenario, the volume-averaged potential temperature between the ρ_1 and ρ_2 surfaces is also unchanged. However, because of the freshening of the subducted water between these two surfaces, the volume-averaged salinity will have decreased. Thus, in this scenario, the surface freshening at constant potential temperature followed by subduction is equivalent to freshening thermocline fluid parcels at a given depth without a change in potential temperature at constant pressure.

On the S – θ diagram ([Fig. A2b](#) ) the freshening and subsequent subduction results in the fluid properties of the

thermocline moving from S_4 to S_5 , and the new water masses along constant density surfaces are both cooler and fresher than the original thermocline properties S_6, θ_6 . Thus, along density surfaces, pure freshening has qualitatively the same effect as pure warming. However, the relationships between these changes along density surfaces to the changes at constant depth are different. It is these differences that provide the basis for distinguishing between the three processes.

c. Pure heave

The pure warming and freshening cases assume that the rate of subduction of fluid into the ocean interior between any two density surfaces remains unchanged. In the case of pure heave the position of density surfaces is allowed to vary, but with no change of water mass properties. Such changes in the position of the density surfaces can occur either as a variation in the rate of subduction or as a response to forced or free waves driven by changes in wind stress curl or by mesoscale variations. Experience has shown that on seasonal timescales the variations of subsurface temperature and salinity are chiefly the result of pure heave ([Bindoff and McDougall 1994](#)), presumably a response to variations in the seasonal wind forcing.

d. Relationships among the observed variables for the three processes

Our starting point is the equations used for translating from observations on height surfaces (i.e., up is positive) to isopycnals. For potential temperature and salinity these equations are (for a detailed discussion see [Bindoff and McDougall 1994](#))

$$\theta'_z = \theta'_n - N'\theta'_z, \quad S'_z = S'_n - N'S'_z, \quad (\text{A1})$$

where N' is the change in the height of a neutral density surface, θ'_z is the change in potential temperature at constant height, and θ'_n is the change in potential temperature along neutral density surfaces.

The definitions of the thermal expansion and haline contraction coefficients, α and β are

$$\alpha = -\frac{1}{\rho} \frac{\partial \rho}{\partial \theta} \Big|_{S,p}, \quad \beta = -\frac{1}{\rho} \frac{\partial \rho}{\partial S} \Big|_{\theta,p} \quad (\text{A2})$$

and from the definition of the neutral surface ([McDougall 1987](#)) we have $\alpha\theta'_n = \beta S'_n$. The vertical gradients of potential temperature and salinity define the stability ratio $R_\rho: \alpha\theta'_z = R_\rho\beta S'_z$.

Given these definitions the three subduction processes can be expressed in terms of the observed variables $S'_z, \theta'_z, S'_n, \theta'_n$, and N' . For pure warming, and making use of the above equations, we get

$$\begin{aligned} \beta S'_z &= 0, & \beta S'_n &= N'\beta S'_z, \\ \frac{\alpha\theta'_n}{\alpha\theta'_z} &= -(R_\rho - 1)^{-1}. \end{aligned} \quad (\text{A3})$$

For pure freshening where the potential temperature is unchanged on pressure surfaces, we get

$$\begin{aligned} \alpha\theta'_z &= 0, & \alpha\theta'_n &= N'\alpha\theta'_z, \\ \frac{\beta S'_n}{\beta S'_z} &= -(1 - R_\rho^{-1})^{-1}. \end{aligned} \quad (\text{A4})$$

For pure heave, where the potential temperature and salinity are unchanged on neutral surfaces we get

$$\alpha\theta'_n = \beta S'_n = 0, \quad \beta S'_z = -N'\beta S'_z, \quad \alpha\theta'_z = -N'\alpha\theta'_z. \quad (\text{A5})$$

For heave we have chosen the sign of strength of this process to be positive where steric height change is positive and neutral surfaces move downward through the water column.

The last three equations, which describe the warming, freshening, and heave processes, can be written as a simple matrix form in terms of the unknown subduction coefficients $[A^w, A^f, A^h]$ and the six “observable” quantities $\alpha\theta'|_z$, $\alpha\theta'|_n$, $N'\alpha\theta_z$, $\beta S'|_z$, $\beta S'|_n$, and $N'\beta S_z$ as

$$\frac{\rho^{-1}\rho'|_z}{R_\rho - 1} \begin{bmatrix} -(R_\rho - 1) & 0 & -R_\rho \\ 1 & R_\rho & 0 \\ R_\rho & R_\rho & R_\rho \\ 0 & (R_\rho - 1) & -1 \\ 1 & R_\rho & 0 \\ 1 & 1 & 1 \end{bmatrix} \begin{bmatrix} A^w \\ A^f \\ A^h \end{bmatrix} = \begin{bmatrix} \alpha\theta'|_z \\ \alpha\theta'|_n \\ N'\alpha\theta_z \\ \beta S'|_z \\ \beta S'|_n \\ N'\beta S_z \end{bmatrix}, \quad (\text{A6})$$

where $[A^w, A^f, A^h]$ are dimensionless and represent the strength of each process.

The above system of equations is rank deficient, with only two nonzero eigenvalues. This rank deficiency can easily be seen by inspecting the rows for linear dependence. The rank deficiency of this system of equations comes about because the observables $\alpha\theta'|_z$, $\alpha\theta'|_n$, $N'\alpha\theta_z$, $\beta S'|_z$, $\beta S'|_n$, $N'\beta S_z$ are dependent on each other. The term $\alpha\theta'|_z$ through [Eq. \(A1\)](#) is dependent on the change in temperature on the neutral surfaces and the vertical excursion of the surface through the mean vertical temperature gradient. The definition of a neutral surface links the variations in time of the temperature on neutral surfaces to the variations salinity on neutral surfaces. Similarly, the definition of R_ρ links the vertical gradients of temperature and salinity to each other. Consequently, through the use of [Eq. \(A1\)](#) and the definition of R_ρ we have reduced the independent information in the observables from six to two.

The weighting of the three processes in [Eq. \(A6\)](#) has been deliberately chosen so that each process has equal importance in contributing to sea level.

APPENDIX B

8. Special Case of Salinity Extrema on the Three Processes

The previous appendix has described a mathematical approach for estimating the strength of the three processes for any arbitrary γ^n surface. Here we focus on the very special case of extrema in salinity on the S - θ curve. At either a salinity minimum or maximum the vertical gradient in salinity is, by definition, zero. The direct result of this is that the pure warming process [[Eq. \(A3\)](#)] can be simplified to $\beta S'|_z = 0$, $\beta S'|_n = 0$, $\theta'|_n = 0$, and $\theta'|_z = -N'\alpha\theta_z$. If one compares these relations with those for the pure heave process at the salinity minimum, it can be seen that pure warming and pure heave have exactly the same relations. These two processes have the precisely same signature in the observations. This degeneracy of the pure heave and pure warming processes has the advantage that it is possible to combine them into a single process and solve the evenly determined system of equations consisting of the two combined processes and pure freshening.

A similar degeneracy also occurs in regions where the vertical gradient of potential temperature is also zero. In this case, pure freshening and heave collapse into a single process and pure warming is well resolved.

Tables

Table 1. The major water masses in the Indian Ocean section, their range of neutral density γ^n , mean depth, potential temperature, salinity, the process that best explains the observed changes, corresponding density regime (I or II) and equivalent

σ_θ . See text for discussion of the Process and Regime columns.

Water mass	γ^n	Depth (bar)	θ (°C)	Salinity	Process	Regime	σ_θ
SAMW	26.7-27.1	410-430	6-14		Warming	I	26.62-26.98
SAW	27.45	1000	4-6	34.47	Freshening	II	27.3
BDW	27.77	1800	3.0	34.62	Heave		27.6
ICDW	27.98	2700	1.29	34.76	Heave		27.79

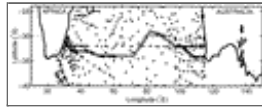
[Click on thumbnail for full-sized image.](#)

Table 2. The relationship between neutral surface density γ^n and σ_θ , σ_1 and σ_2 . The linear relationship is given by $\sigma_\theta = a(\gamma^n - 26.5) + b$ where a is the slope and b is the intercept at $\gamma^n = 26.5$; R^2 is the percentage variance explained by the linear fit between these two density coordinates.

σ	a	b	R^2
σ_θ	0.9125	26.4351	1.000
σ_1	1.0840	30.8526	1.000
σ_2	1.2488	35.1805	1.000

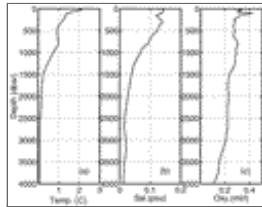
[Click on thumbnail for full-sized image.](#)

Figures



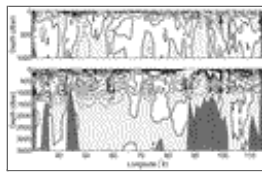
[Click on thumbnail for full-sized image.](#)

Fig. 1. The hydrographic data collected by the RRS *Charles Darwin* in 1987 (shown by circles) and the historical data (median date 1962) used for this analysis (shown by crosses)



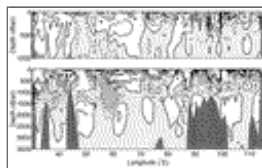
[Click on thumbnail for full-sized image.](#)

Fig. 2. The estimates of the a priori noise from the historical data for each of the three variables (a) temperature, (b) salinity, and (c) oxygen.



[Click on thumbnail for full-sized image.](#)

Fig. 3. Temperature differences (°C) between the austral spring of 1987 and the historical temperature data on isobars (median date 1962). Positive differences, shown by continuous lines, denote warmer temperatures in 1987 compared to 1962. Note different contour levels for each panel.



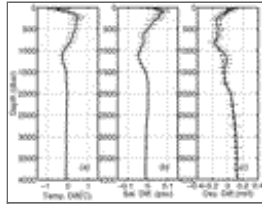
[Click on thumbnail for full-sized image.](#)

Fig. 4. As in [Fig. 3](#) except for salinity (psu).



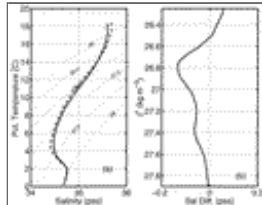
Click on thumbnail for full-sized image.

Fig. 5. As in Fig. 3 except for oxygen (ml L^{-1}).



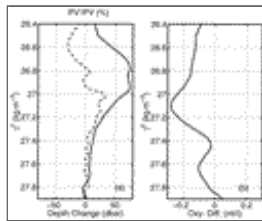
Click on thumbnail for full-sized image.

Fig. 6. The difference of temperature (a), salinity (b), and oxygen (c) averaged along isobars across the Indian Ocean between the 1987 data and 1962 historical data. The dashed line in (c) is the oxygen difference on isobars that would have occurred if there had been no change in temperature on isobars. This line is estimated using the observed temperature difference shown in (a) to remove the effect of changes in oxygen saturation due to temperature changes. The horizontal bars are 90% confidence intervals (see text).



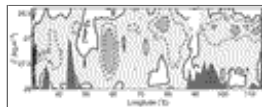
Click on thumbnail for full-sized image.

Fig. 7. (a) Average $S-\theta$ curves for the 1987 hydrographic data (dashed line) and the 1962 mapped historical data (continuous line) and (b) the average salinity difference between 1987 and 1962 data along neutral surfaces (γ^n). Negative differences indicate that on neutral surfaces the salinity is fresher in 1987. On (a) the lines of constant γ^n are based on the nearly linear relationship between σ_θ and γ^n .



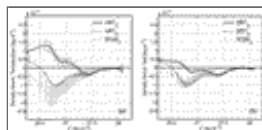
Click on thumbnail for full-sized image.

Fig. 8. (a) Average pressure difference along neutral surfaces (γ^n) for the 1962 historical data and the 1987 data (continuous line) and the percentage PV change ($=-h'/h$), where h is the average distance between neutral surfaces (dashed line) and (b) the average oxygen difference along neutral surfaces (γ^n) for Cruise 29 and the mapped historical data. Positive differences indicate the isopycnals are deeper, have more vorticity, or are higher in oxygen concentration in 1987.



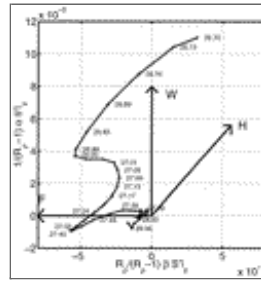
Click on thumbnail for full-sized image.

Fig. 9. The difference in potential temperature between 1987 data and the 1962 mapped historical data on neutral surfaces across the Indian Ocean. Positive differences imply an increase in neutral surface temperature. Contour intervals are in degrees Celsius.



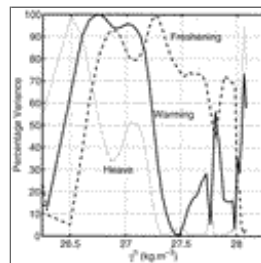
Click on thumbnail for full-sized image.

Fig. 10. Graphs of the zonal average of $\alpha\theta'_z$, $\alpha\theta'_n$, $N'\alpha\theta'_z$, $\beta S'_z$, $\beta S'_n$, and $N'\beta S'_z$ as a function of neutral density γ^n between the 1987 data and the 1962 historical data. The continuous, dashed, and dotted lines in (a) correspond to $\alpha\theta'_z$, $\alpha\theta'_n$, $N'\alpha\theta'_z$ and in (b) to $\beta S'_z$, $\beta S'_n$, and $N'\beta S'_z$. The vertical bars are 90% confidence intervals for each variable.



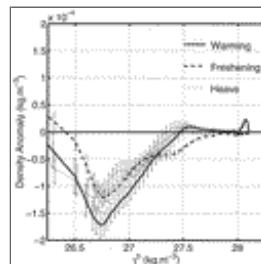
Click on thumbnail for full-sized image.

Fig. 11. Graphs of $R_\rho / (R_\rho - 1) \beta S'_z$ against $1 / (R_\rho - 1) \alpha \theta'_z$ as a function of neutral density. A subset of the neutral density surfaces γ^n (in kg m^{-3}) are labeled on this hodograph. The vectors starting from the origin and labeled **W**, **F**, and **H** are, respectively, the directions that pure warming, pure freshening, and pure heave have. Points on the hodograph represent vectors drawn from the origin.



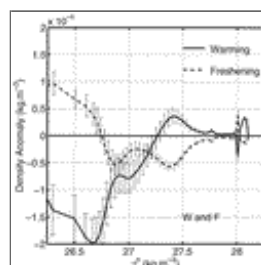
Click on thumbnail for full-sized image.

Fig. 12. The variance explained for the case of (i) pure warming alone (continuous line), (ii) pure freshening alone (dashed line), and (iii) pure heave alone (dotted line) for the differences between the 1987 data and 1962 historical data.



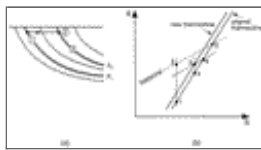
Click on thumbnail for full-sized image.

Fig. 13. The average density anomaly, $\rho^{-1} \rho'_z$, as a function of a neutral surface across the Indian Ocean for the case of (i) pure warming alone (continuous line), (ii) pure freshening alone (dashed line), and (iii) pure heave alone (dotted line). The average density anomaly is the contribution of sea-level change by each process on each neutral surface. The vertical bars are 90% confidence intervals for each process.



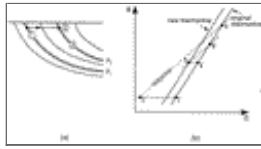
Click on thumbnail for full-sized image.

Fig. 14. The average density anomaly, $\rho^{-1} \rho'_z$, as a function of neutral surface γ^n across the Indian Ocean for the case where both warming and freshening are retained in [Eq. \(A6\)](#), making an evenly determined system. The continuous and dashed lines are, respectively, the warming and freshening response. The vertical bars are 90% confidence intervals for each process.



[Click on thumbnail for full-sized image.](#)

Fig. A1. The pure warming process (a) in physical space and (b) in $S-\theta$ space. See text in appendix A for a complete description.



[Click on thumbnail for full-sized image.](#)

Fig. A2. As in [Fig. A1](#) except for the pure freshening process.

Corresponding author address: Dr. Nathan Bindoff, Antarctic CRC, University of Tasmania, GPO Box 252-80, Hobart, Tasmania 7001, Australia.

E-mail: n.bindoff@utas.edu.au

[top ▲](#)



© 2008 American Meteorological Society [Privacy Policy and Disclaimer](#)
 Headquarters: 45 Beacon Street Boston, MA 02108-3693
 DC Office: 1120 G Street, NW, Suite 800 Washington DC, 20005-3826
amsinfo@ametsoc.org Phone: 617-227-2425 Fax: 617-742-8718
[Allen Press, Inc.](#) assists in the online publication of *AMS* journals.